Bergische Universität Wuppertal

Fachbereich Mathematik und Naturwissenschaften

Lehrstuhl für Angewandte Mathematik
und Numerische Mathematik

Roland Pulch

Finite Difference Methods for Solving Warped Multirate Partial Differential Algebraic Equations

June 2004

http://www.math.uni-wuppertal.de/org/Num/

Finite Difference Methods for Solving Warped Multirate Partial Differential Algebraic Equations

R. Pulch

Bergische Universität Wuppertal, Fachbereich Mathematik und Naturwissenschaften, Lehrstuhl für Angewandte Mathematik und Numerische Mathematik, Gaußstr. 20, D-42119 Wuppertal, Germany.

Abstract

In communication electronics, circuits often generate high frequency signals, whose amplitude and frequency are modulated by a slowly varying signal. A multidimensional approach offers an efficient strategy for numerical simulation by modelling the circuit via a warped multirate partial differential algebraic equation (PDAE). The arising periodic boundary value problem can be solved directly by conventional finite difference methods on uniform grids. On the other hand, the PDAE system exhibits an information transport along characteristic curves. We apply this inherent structure to design a sophisticated finite difference method on characteristic grids. Accordingly, this technique yields drastic savings in computation time and memory. Numerical simulations using a benchmark problem verify this efficiency by a comparison between a uniform and a characteristic grid scheme.

1   Introduction

The mathematical modelling of electric circuits uses a network approach [7], which yields systems of differential algebraic equations (DAEs). Thereby, the system describes the transient behaviour of all node voltages and some branch currents. In communication electronics, the corresponding solutions often represent high frequency oscillations, where amplitude and form change slowly in time. Applying a numerical integration scheme, the fastest time rate restricts the step

sizes, whereas the slowest rate specifies the total time interval. Thus if the time scales are widely separated, then transient analysis of the DAE system becomes inefficient.

Alternatively, a multidimensional model can be applied to represent such quasi-periodic signals efficiently. Therefore the DAE model generates a multirate partial differential algebraic equation (MPDAE), which was introduced by Brachtendorf et al. and successfully simulated in frequency domain [1]. Thereby, the time scales are driven by input signals. Multiperiodic solutions of the partial system yield quasiperiodic DAE solutions. General time domain methods are also feasible for the MPDAE system [16]. In particular, the MPDAE implies an information transport along characteristic curves [12]. Using this inherent structure, capable time domain techniques can be constructed for solving the periodic boundary value problems [13]. The efficient solution of the MPDAE system is crucial to compete with the DAE model.

The presence of autonomous time scales in addition to driven rates permits frequency modulation. Consequently, the multidimensional model was generalised to this situation by Narayan and Roychowdhury [11], where a warped MPDAE system arises. Now a local frequency function has to be determined in addition to the multiperiodic solution. This feature causes theoretical and numerical problems, since appropriate conditions are needed to ensure the existence and uniqueness of solutions.

The warped MPDAE system also includes a respective information transport. However, the characteristic projections depend on the unknown local frequency function now. Nevertheless, time domain methods can be developed, which perform an integration along the characteristic curves, too. In the case of an underlying ordinary differential equation, shooting methods successfully solve the arising boundary value problems of the characteristic systems [14].

In this paper, we construct an according finite difference method for solving the boundary value problems of the characteristic systems. This scheme can be applied directly to the DAE case. In contrast to finite difference methods on uniform grids, the local frequencies specify the position of the grid points now. Thus the location of the grid is a priori unknown, which demands a sophisticated implementation of this technique. On the other hand, the arising nonlinear system is much less coupled, since it regards the inherent structure of the MPDAE, whereas uniform grids include an inappropriate coupling in all coordinate directions. Consequently, the amount of computation time and memory reduces drastically in the corresponding Newton iterations, because the LU decompositions of the large linear systems remain sparse.

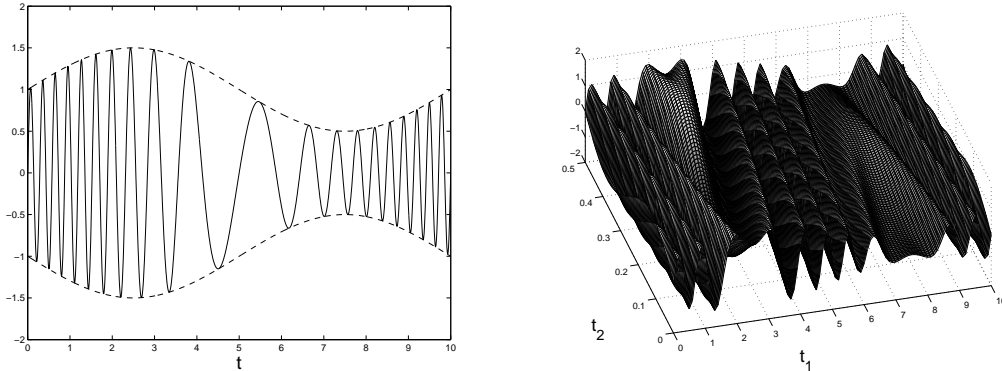The paper is organised as follows. We describe the multidimensional signal model

Figure 1: Frequency modulated signal x and unsophisticated MVF $\hat{x}_1$.

and the resulting warped MPDAE model in Sect. 2 and Sect. 3, respectively. Then a finite difference method using a uniform grid is introduced for comparison. In Sect. 5, we construct a finite difference method, which is based on the information transport along the characteristic curves. Finally, a Van der Pol oscillator in DAE formulation provides a benchmark to present numerical simulations and to compare the efficiency of the two described techniques.

2 Multidimensional Signal Model

We analyse multitone signals, which include amplitude modulation as well as frequency modulation. A simple example is the function

$$x(t) = \left[1 + \alpha \sin\left(\tfrac{2\pi}{T_1}t\right)\right] \sin\left(\tfrac{2\pi}{T_2}t + \beta \sin\left(\tfrac{2\pi}{T_1}t\right)\right) \tag{1}$$

with the time scales $T_1 \gg T_2$. Hence we obtain a high frequency oscillation with fast rate T_2. The parameter $0 < \alpha < 1$ implies the amplitude modulation, whereas the parameter $\beta > 0$ determines the frequency modulation. Changes in time during the slower rate T_1 produce these two variations. Accordingly, we require many time steps to capture all fast oscillations within the slow modulation. Fig. 1 illustrates the signal (1) qualitatively.

Alternatively, we assign an own variable to each separate time scale. Thus our example suggests the multidimensional model

$$\hat{x}_1(t_1, t_2) = \left[1 + \alpha \sin\left(\tfrac{2\pi}{T_1}t_1\right)\right] \sin\left(\tfrac{2\pi}{T_2}t_2 + \beta \sin\left(\tfrac{2\pi}{T_1}t_1\right)\right), \tag{2}$$

which is called the *multivariate function* (*MVF*) of the signal (1). Since the time scales are decoupled now, the representation (2) is biperiodic and therefore al-
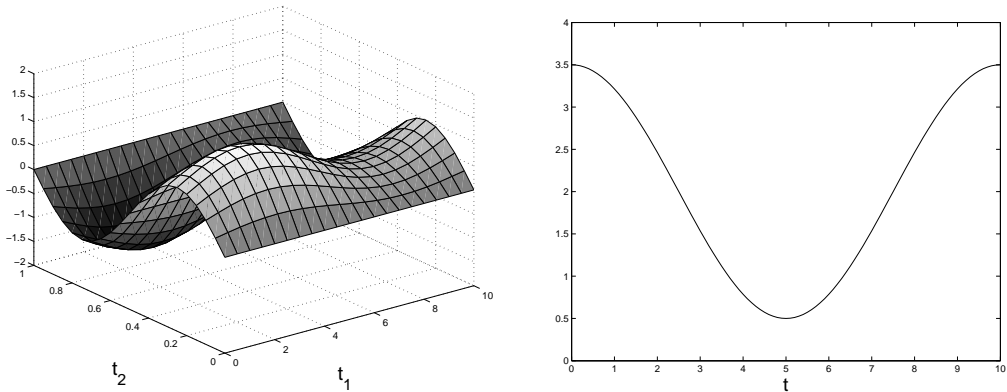
3

Figure 2: MVF $\hat{x}_2$ and corresponding local frequency ν.

ready fixed by its values in the rectangle $[0, T_1[\times [0, T_2[$. We are able to reconstruct the multitone signal completely by its MVF using

$$x(t) = \hat{x}_1(t, t). \tag{3}$$

In general, this strategy produces simple MVFs for purely amplitude modulated signals. However, frequency modulation may lead to inefficient representations. Fig. 1 also shows the MVF (2), which includes many oscillations, too. The number of oscillations increases, the larger the amount of frequency modulation β becomes.

To avoid this phenomenon, Narayan and Roychowdhury [11] recommend to model the frequency modulation separately. Thus the MVF just includes the amplitude modulation part. Our example yields the representation

$$\hat{x}_2(t_1, t_2) = \left[1 + \alpha \sin \left(\tfrac{2\pi}{T_1} t_1 \right) \right] \sin \left(2\pi t_2 \right), \tag{4}$$

where the second period is transformed to 1. The frequency modulation part is included in the *warping function*

$$\Psi(t) = \frac{t}{T_2} + \frac{\beta}{2\pi} \sin \left(\tfrac{2\pi}{T_1} t \right), \tag{5}$$

which stretches the second time scale. We define the *local frequency* ν of the signal (1) by $\nu := \Psi'$, which results in the T_1-periodic function

$$\nu(t) = \frac{1}{T_2} + \frac{\beta}{T_1} \cos \left(\tfrac{2\pi}{T_1} t \right). \tag{6}$$

Fig. 2 illustrates the MVF (4) and the local frequency (6). Both functions have a simple behaviour now and thus the new representation is efficient. We reconstruct the multitone signal (1) via

$$x(t) = \hat{x}_2(t, \Psi(t)). \tag{7}$$

4

The multidimensional model can be applied for any frequency modulated quasi-periodic signal $\mathbf{x}(t) \in \mathbb{R}^n$ of the form

$$\mathbf{x}(t) = \sum_{j_1,j_2=-\infty}^{\infty} \mathbf{X}_{j_1,j_2} \exp\left(i\left(\tfrac{2\pi}{T_1}j_1 t + 2\pi j_2 \Psi(t)\right)\right) \tag{8}$$

with constant coefficients $\mathbf{X}_{j_1,j_2} \in \mathbb{C}^n$ and warping function $\Psi(t) \in \mathbb{R}$. We assume absolute convergence in the series of the representation (8).

3 Warped Multirate PDAE

To model electric circuits mathematically, a network approach is used [3], which typically yields systems of *differential algebraic equations* (*DAEs*). These systems cause theoretical and numerical problems indicated by the index concept and the need of consistent values [4]. We write such a DAE system in the form

$$\tfrac{d}{dt}\mathbf{q}(\mathbf{x}) = \mathbf{f}(\mathbf{x}(t)) + \mathbf{b}(t), \tag{9}$$

where $\mathbf{x}: \mathbb{R} \to \mathbb{R}^k$ denotes unknown voltages and currents. The Jacobian matrix of the function $\mathbf{q}: \mathbb{R}^k \to \mathbb{R}^k$ is singular in general. The right-hand side includes the function $\mathbf{f}: \mathbb{R}^k \to \mathbb{R}^k$ and independent input signals $\mathbf{b}: \mathbb{R} \to \mathbb{R}^k$. Using a constant input $\mathbf{b} \equiv \mathbf{b}_0$, we assume that the DAE (9) has a periodic steady state respond $\mathbf{x}$. Time and frequency domain methods can be used to compute this solution, see [8]. Changing the input slowly in time may modulate the amplitude as well as the frequency of this oscillation. If we apply T_1-periodic input signals $\mathbf{b}$, then solutions $\mathbf{x}$ of the form (8) arise. The period T_1 shall be much larger than the time scales $1/\nu = 1/\Psi'$ of the local frequency.

Under these assumptions, the multidimensional signal model becomes powerful. The transition to MVFs transforms the DAE system (9) into the system

$$\frac{\partial \mathbf{q}(\hat{\mathbf{x}})}{\partial t_1} + \nu(t_1)\frac{\partial \mathbf{q}(\hat{\mathbf{x}})}{\partial t_2} = \mathbf{f}(\hat{\mathbf{x}}(t_1, t_2)) + \mathbf{b}(t_1) \tag{10}$$

with the MVF $\hat{\mathbf{x}}$ of $\mathbf{x}$ and the local frequency ν, whereas $\mathbf{q}, \mathbf{f}, \mathbf{b}$ remain the same as before. The system (10) is called the *warped multirate partial differential algebraic equation* (*MPDAE*) corresponding to the DAE (9). If a $(T_1, 1)$-periodic MVF $\hat{\mathbf{x}}$ satisfies the MPDAE with T_1-periodic local frequency ν, then the reconstruction (7) yields a solution $\mathbf{x}$ of the DAE owning the form (8).

We have to choose a local frequency ν, which yields an efficient MVF representation. However, there is no a priori knowledge how to fix this function appropriately. Hence we handle the local frequency as an additional unknown function

and pose an extra condition to obtain a well determined system. The specification of a suitable requirement represents yet another problem [5, 11]. In time domain, the additional boundary condition

$$\frac{\partial \hat{\mathbf{x}}^1}{\partial t_2}(t_1, 0) = 0 \quad \text{for all } t_1 \in [0, T_1[\tag{11}$$

in just one component of $\hat{\mathbf{x}}$, without loss of generality the first component here, turns out to be a successful choice [14]. We will use the phase condition (11) in the following.

Thus the efficiency of the multidimensional model depends on qualified methods for solving biperiodic boundary value problems. In this paper, we consider semi-explicit DAEs of the form

$$
\begin{aligned}
\frac{d}{dt}\mathbf{x}^d &= \mathbf{f}^d(\mathbf{x}^d(t), \mathbf{x}^a(t)) + \mathbf{b}^d(t) \\
\mathbf{0} &= \mathbf{f}^a(\mathbf{x}^d(t), \mathbf{x}^a(t)) + \mathbf{b}^a(t)
\end{aligned} \tag{12}
$$

with $\mathbf{x}^d, \mathbf{f}^d, \mathbf{b}^d \in \mathbb{R}^{k^d}$ and $\mathbf{x}^a, \mathbf{f}^a, \mathbf{b}^a \in \mathbb{R}^{k^a}$ ($k = k^d + k^a$). We assume a differential index of one, which is equivalent to the regularity of the Jacobian matrix $\frac{\partial \mathbf{f}^a}{\partial \mathbf{x}^a}$ in a neighbourhood of the solution. The corresponding warped MPDAE results in

$$
\begin{aligned}
\frac{\partial \hat{\mathbf{x}}^d}{\partial t_1} + \nu(t_1)\frac{\partial \hat{\mathbf{x}}^d}{\partial t_2} &= \mathbf{f}^d(\hat{\mathbf{x}}^d(t_1, t_2), \hat{\mathbf{x}}^a(t_1, t_2)) + \mathbf{b}^d(t_1) \\
\mathbf{0} &= \mathbf{f}^a(\hat{\mathbf{x}}^d(t_1, t_2), \hat{\mathbf{x}}^a(t_1, t_2)) + \mathbf{b}^a(t_1)
\end{aligned} \tag{13}
$$

with the MVFs $\hat{\mathbf{x}}^d, \hat{\mathbf{x}}^a$. Generalisations of the following methods to the case of higher index DAEs are straightforward.

4 Uniform Grid Method

A standard approach to solve the MPDAE system (13) is to apply a finite difference method. Therefore the partial derivatives are replaced by difference formulae on a grid in time domain. According to the biperiodic boundary conditions, we consider the rectangle $[0, T_1[\times[0, 1[$ and use a uniform grid including the mesh points

$$(t_{1,j_1}, t_{2,j_2}) = ((j_1 - 1)h_1, (j_2 - 1)h_2) \quad \text{with} \quad h_1 = \frac{T_1}{n_1},\ h_2 = \frac{1}{n_2} \tag{14}$$

for $j_1 = 1, \ldots, n_1$; $j_2 = 1, \ldots, n_2$. Fig. 3 outlines this grid in time domain.
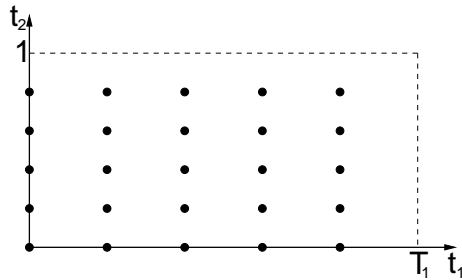
Figure 3: Uniform grid in time domain.

Now we substitute the partial derivatives in (13) by central difference quotients, for example, which yields the nonlinear systems

$$
\begin{aligned}
\tfrac{1}{2h_1} \left[\hat{\mathbf{x}}^d_{j_1+1,j_2} - \hat{\mathbf{x}}^d_{j_1-1,j_2} \right] & \\
+\nu_{j_1} \tfrac{1}{2h_2} \left[\hat{\mathbf{x}}^d_{j_1,j_2+1} - \hat{\mathbf{x}}^d_{j_1,j_2-1} \right] &= \mathbf{f}^d(\hat{\mathbf{x}}^d_{j_1,j_2}, \hat{\mathbf{x}}^a_{j_1,j_2}) + \mathbf{b}^d(t_{1,j_1}) \\
\mathbf{0} &= \mathbf{f}^a(\hat{\mathbf{x}}^d_{j_1,j_2}, \hat{\mathbf{x}}^a_{j_1,j_2}) + \mathbf{b}^a(t_{1,j_1})
\end{aligned}
\tag{15}
$$

for $j_1 = 1, \ldots, n_1$; $j_2 = 1, \ldots, n_2$. Thereby, $\hat{\mathbf{x}}^{d/a}_{j_1,j_2} \in \mathbb{R}^{k^{d/a}}$ represents the approximation of $\hat{\mathbf{x}}^{d/a}$ in the grid point (t_{1,j_1}, t_{2,j_2}) and ν_{j_1} the approximation of ν in t_{1,j_1}. We eliminate the arising unknowns for $j_1 = 0, n_1 + 1$ and $j_2 = 0, n_2 + 1$ directly by using the periodicities. The resulting numerical solution will be biperiodic due to this construction. Consequently, we obtain a nonlinear system of $n_1 n_2 k$ equations for $n_1 n_2 k + n_1$ unknowns.

By means of discretisation, it is easy to include the phase condition (11) in the uniform grid. Using central differences again, we obtain the scalar equations

$$
\tfrac{1}{2h_2} \left[\hat{\mathbf{x}}^{d,1}_{j_1,2} - \hat{\mathbf{x}}^{d,1}_{j_1,n_2} \right] = 0
\tag{16}
$$

in the first component of $\hat{\mathbf{x}}^d$ for $j_1 = 1, \ldots, n_1$. Now the nonlinear systems (15),(16) include as many equations as unknowns. The used difference formulae are all consistent of order two. We can apply methods of Newton type to solve the complete nonlinear system iteratively. This nonlinear system is strongly coupled, because the uniform grid causes a mixture of both coordinate directions.

The Jacobian matrix arising in the linear systems of Newton's method is sparse. Yet a Gaussian elimination produces many new fill-ins in the corresponding LU decomposition due to the strong coupling, which increases the amount of computation work and memory. Certain sparse solvers can reduce the number of fill-ins by permutations of rows and columns. Thereby, accuracy is lost, since the algorithms neglect pivoting for numerical stability. Moreover, the determination of efficient permutations demands large computation times, too. The use

of iterative methods for the linear systems is also doubtful, because the Jacobian matrix is neither symmetric nor positive definite.

5   Characteristic Grid Method

The following analysis and notions correspond to the case of a scalar PDE [6]. Our PDAE system (10) exhibits an information transport along *characteristic curves* [14]. The *characteristic projections*, which are situated in the domain of dependence, do not depend on the unknown solution $\hat{\mathbf{x}}$ but on the unknown local frequency ν. It holds

$$
\begin{aligned}
t_1(\tau) &= \tau + c_1 \\
t_2(\tau) &= \Psi(t_1) + c_2 \quad \text{with} \quad \Psi(t_1) = \int_0^{t_1} \nu(\tau)\, d\tau
\end{aligned}
\tag{17}
$$

with a parameter $\tau \in \mathbb{R}$ and arbitrary integration constants $c_1, c_2 \in \mathbb{R}$. Thus the characteristic projections (17) represent a continuum of parallel curves.

The special system (13) includes the same continuum. On each characteristic projection, we obtain the *characteristic system*

$$
\begin{aligned}
\tfrac{d}{d\tau}\tilde{\mathbf{x}}^d &= \mathbf{f}^d(\tilde{\mathbf{x}}^d(\tau), \tilde{\mathbf{x}}^a(\tau)) + \mathbf{b}^d(\tau + c_1) \\
\mathbf{0} &= \mathbf{f}^a(\tilde{\mathbf{x}}^d(\tau), \tilde{\mathbf{x}}^a(\tau)) + \mathbf{b}^a(\tau + c_1),
\end{aligned}
\tag{18}
$$

where the solution $\tilde{\mathbf{x}}^{d/a}$ depends on the parameter τ. The system (18) has the same form as the original DAE (12).

Due to the periodicities, we consider the rectangle $[0, T_1[\times [0, 1[$ again. From the continuum (17), we choose the n_1 projections starting in the initial points $(t_{1,j_1}^{ini}, 0)$ for $j_1 = 1, \ldots, n_1$ with $t_{1,j_1}^{ini} = (j_1 - 1)h_1$ and $h_1 = \frac{T_1}{n_1}$, i.e.

$$
\begin{aligned}
t_1(\tau) &= \tau + t_{1,j_1}^{ini} \\
t_2(\tau) &= \Psi(\tau + t_{1,j_1}^{ini}) - \Psi(t_{1,j_1}^{ini}) = \int_{t_{1,j_1}^{ini}}^{\tau + t_{1,j_1}^{ini}} \nu(\sigma)\, d\sigma.
\end{aligned}
\tag{19}
$$

Fig. 4 sketches this selection. Accordingly, we obtain the n_1 systems

$$
\begin{aligned}
\tfrac{d}{d\tau}\tilde{\mathbf{x}}_{j_1}^d &= \mathbf{f}^d(\tilde{\mathbf{x}}_{j_1}^d(\tau), \tilde{\mathbf{x}}_{j_1}^a(\tau)) + \mathbf{b}^d(\tau + t_{1,j_1}^{ini}) \\
\mathbf{0} &= \mathbf{f}^a(\tilde{\mathbf{x}}_{j_1}^d(\tau), \tilde{\mathbf{x}}_{j_1}^a(\tau)) + \mathbf{b}^a(\tau + t_{1,j_1}^{ini})
\end{aligned}
\tag{20}
$$

for the functions $\tilde{\mathbf{x}}_{j_1}^{d/a}$ on each characteristic projection. This strategy is similar to a semi-discretisation, since we select a finite number of characteristic curves of the MPDAE system to produce a system of DAE subsystems.
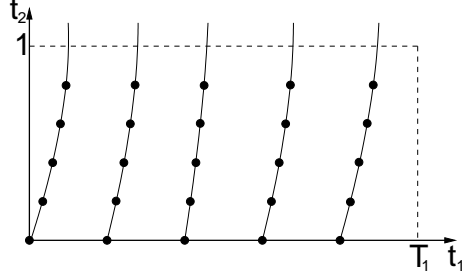
8

Figure 4: Characteristic grid in time domain.

We assume that the local frequency ν is T_1-periodic and positive, which yields a bijective warping function Ψ. Hence the characteristic projection running through the j_1th initial value intersects the line $t_2 = 1$ at the end point

$$(t_{1,j_1}^{end}, 1) = (\Psi^{-1}(\Psi(t_{1,j_1}^{ini}) + 1), 1). \tag{21}$$

It follows that the time interval $[0, \tau_{j_1}]$ for the integration on the j_1th characteristic curve has the length

$$\tau_{j_1} = t_{1,j_1}^{end} - t_{1,j_1}^{ini} = \Psi^{-1}(\Psi(t_{1,j_1}^{ini}) + 1) - t_{1,j_1}^{ini}. \tag{22}$$

Moreover, since we consider widely separated time scales $1/\nu(t_1) \ll T_1$, let $1/\nu(t_1) < h_1$ for all t_1. It follows $t_{1,j_1}^{ini} < t_{1,j_1}^{end} < t_{1,j_1+1}^{ini}$ and $0 < \tau_{j_1} < h_1$ for all j_1. Since the local frequency is unknown, we discretise this function to obtain the n_1 values $\nu_{j_1} = \nu(t_{1,j_1}^{ini})$. Given starting values ν_{j_1}, we can approximate the function Ψ in (19) by numerical integration. For example, using trapezoidal rule yields

$$t_2(\tau) = \int_{t_{1,j_1}^{ini}}^{\tau + t_{1,j_1}^{ini}} \nu(\sigma) \, d\sigma \doteq \left(\tau - \frac{\tau^2}{2h_1}\right) \nu_{j_1} + \frac{\tau^2}{2h_1} \nu_{j_1+1}, \tag{23}$$

which corresponds to fit the characteristic projections by quadratic polynomials. Hence we obtain an approximation of the interval length (22) by means of this polynomial.

The periodicity in the second coordinate provides boundary conditions for the functions $\tilde{\mathbf{x}}_{j_1}^d$ in the systems (20). We approximate the end values by the initial values using, for example, linear interpolation with two neighbouring points

$$
\begin{aligned}
\tilde{\mathbf{x}}_{j_1}^d(\tau_{j_1}) &= \hat{\mathbf{x}}^d(t_{1,j_1}^{end}, 1) = \hat{\mathbf{x}}^d(t_{1,j_1}^{end}, 0) \\
&\doteq \left(1 - \tfrac{\tau_{j_1}}{h_1}\right) \hat{\mathbf{x}}^d(t_{1,j_1}^{ini}, 0) + \tfrac{\tau_{j_1}}{h_1} \hat{\mathbf{x}}^d(t_{1,j_1+1}^{ini}, 0) \\
&= \left(1 - \tfrac{\tau_{j_1}}{h_1}\right) \tilde{\mathbf{x}}_{j_1}^d(0) + \tfrac{\tau_{j_1}}{h_1} \tilde{\mathbf{x}}_{j_1+1}^d(0)
\end{aligned}
\tag{24}
$$

9

for $j_1 = 1, \ldots, n_1$, where $j_1 = n_1 + 1$ is identified with $j_1 = 1$ due to the periodicity in the first coordinate. Hence we obtain linear boundary conditions, which are consistent of order two. On the other hand, the functions $\tilde{\mathbf{x}}_{j_1}^a$ depend on the components $\tilde{\mathbf{x}}_{j_1}^d$. Consequently, we do not interpolate the corresponding end values, but add the algebraic constraints to the boundary conditions, i.e.

$$0 = \mathbf{f}^a(\tilde{\mathbf{x}}_{j_1}^d(0), \tilde{\mathbf{x}}_{j_1}^a(0)) + \mathbf{b}^a(t_{1,j_1}^{ini}) \qquad (25)$$

for $j_1 = 1, \ldots, n_1$.

The union of all equations (20),(24),(25) for $j_1 = 1, \ldots, n_1$ represents a free boundary value problem of $n_1 k$ DAEs for $n_1 k$ unknown functions. The subsystems (20) refer to separate characteristic projections and thus they are coupled by the boundary conditions (24) only. This degree of independence causes the reduction in the computational work. Furthermore, an inherent potential for parallelism originates by this construction.

The scalar unknowns $\tau_1, \ldots, \tau_{n_1}$ are determined by additional conditions. The phase condition (11) can not be included directly, since the characteristic curves do not start exactly in t_2-direction. However, we use the first equation of the MPDAE, where the derivative with respect to t_1 is replaced by the central difference quotient, and obtain the formulae

$$\mathbf{f}^{d,1}(\tilde{\mathbf{x}}_{j_1}^d(0), \tilde{\mathbf{x}}_{j_1}^a(0)) + \mathbf{b}^{d,1}(t_{1,j_1}^{ini}) - \frac{1}{2h_1}\left[\tilde{\mathbf{x}}_{j_1+1}^{d,1}(0) - \tilde{\mathbf{x}}_{j_1-1}^{d,1}(0)\right] = 0 \qquad (26)$$

for $j_1 = 1, \ldots, n_1$. Regarding the periodicity in t_1-direction, these conditions just involve unknown initial values and we add them to the boundary conditions.

A numerical solution of the complete boundary value problem yields an approximation of the biperiodic MPDAE solution in the observed time domain rectangle. Shooting methods are feasible to solve DAE boundary value problems, see [2, 9]. In our application, shooting methods have been successfully used in the case of an underlying ODE system, where a free boundary value problem of ODEs arises [14].

Alternatively, we solve the problem (20),(24),(25),(26) by a finite difference technique now. In contrast to shooting methods, we omit a forward integration of the DAEs, where the sensitivities on independent initial values have to be computed appropriately. This fact allows an easy implementation and causes more robustness in general. Therefore the DAE systems (20) are discretised on a characteristic grid, which lies on the separate characteristic projections, see Fig. 4. Each of the intervals $[0, \tau_{j_1}]$ can be divided adaptively. For simplicity, we may choose an equidistant step size in t_2-direction yielding the grid points

$$(t_{1,j_1,j_2}^{(I)}, t_{2,j_2}^{(I)}) = (\Psi^{-1}(\Psi((j_1-1)h_1) + (j_2-1)h_2), (j_2-1)h_2) \qquad (27)$$

10

with $h_1 = \frac{T_1}{n_1}$, $h_2 = \frac{1}{n_2}$ for $j_1 = 1, \ldots, n_1$; $j_2 = 1, \ldots, n_2$. Another feasible choice is to apply equidistant step size in t_1-direction, which produces the grid points

$$
\begin{aligned}
(t^{(II)}_{1,j_1,j_2}, t^{(II)}_{2,j_1,j_2}) &= ((j_1 - 1)h_1 + (j_2 - 1)h_2\tau_{j_1}, \\
&\qquad \Psi((j_1 - 1)h_1 + (j_2 - 1)h_2\tau_{j_1}) - \Psi((j_1 - 1)h_1))
\end{aligned} \tag{28}
$$

for $j_1 = 1, \ldots, n_1$; $j_2 = 1, \ldots, n_2$.

By a discretisation of the whole MPDAE (13) like in the previous section, difference formulae can just replace the derivatives. In the systems (20), we also have the possibility to choose a numerical integration scheme. For example, we select the trapezoidal rule, which is consistent of order two. Consequently, just two successive grid points are coupled by the formula, whereas the uniform grid demands a stronger coupling to achieve an order of two. We apply the trapezoidal rule to the semi-explicit DAEs via an indirect approach [15] and obtain the nonlinear systems

$$
\begin{aligned}
\tilde{\mathbf{x}}^d_{j_1,j_2+1} - \tilde{\mathbf{x}}^d_{j_1,j_2} &= \tfrac{1}{2}(t_{1,j_1,j_2+1} - t_{1,j_1,j_2})\left[\mathbf{f}^d(\tilde{\mathbf{x}}^d_{j_1,j_2}, \tilde{\mathbf{x}}^a_{j_1,j_2}) + \mathbf{b}^d(t_{1,j_1,j_2}) \right. \\
&\qquad\qquad \left. + \mathbf{f}^d(\tilde{\mathbf{x}}^d_{j_1,j_2+1}, \tilde{\mathbf{x}}^a_{j_1,j_2+1}) + \mathbf{b}^d(t_{1,j_1,j_2+1})\right] \quad (29) \\
\mathbf{0} &= \mathbf{f}^a(\tilde{\mathbf{x}}^d_{j_1,j_2}, \tilde{\mathbf{x}}^a_{j_1,j_2}) + \mathbf{b}^a(t_{1,j_1,j_2})
\end{aligned}
$$

for $j_1 = 1, \ldots, n_1$; $j_2 = 1, \ldots, n_2$, where $\tilde{\mathbf{x}}^{d/a}_{j_1,j_2}$ represents the approximation in the corresponding grid point. The values t_{1,j_1,j_2} may be chosen from either (27) or (28). Following (24), the unknowns for $j_2 = n_2 + 1$ on the left-hand side can be substituted by

$$
\tilde{\mathbf{x}}^d_{j_1,n_2+1} = \left(1 - \frac{\tau_{j_1}}{h_1}\right)\tilde{\mathbf{x}}^d_{j_1,1} + \frac{\tau_{j_1}}{h_1}\tilde{\mathbf{x}}^d_{j_1+1,1} \tag{30}
$$

and the according function evaluation by

$$
\mathbf{f}^d(\tilde{\mathbf{x}}^d_{j_1,n_2+1}, \tilde{\mathbf{x}}^a_{j_1,n_2+1}) = \left(1 - \frac{\tau_{j_1}}{h_1}\right)\mathbf{f}^d(\tilde{\mathbf{x}}^d_{j_1,1}, \tilde{\mathbf{x}}^a_{j_1,1}) + \frac{\tau_{j_1}}{h_1}\mathbf{f}^d(\tilde{\mathbf{x}}^d_{j_1+1,1}, \tilde{\mathbf{x}}^a_{j_1+1,1}), \tag{31}
$$

which saves evaluations in comparison to using (30) for $\tilde{\mathbf{x}}^{d/a}_{j_1,n_2+1}$ and inserting it into $\mathbf{f}^d$. The algebraic boundary conditions (25) are already included in the systems (29). Finally, we add the phase conditions (26)

$$
\mathbf{f}^{d,1}(\tilde{\mathbf{x}}^d_{j_1,1}, \tilde{\mathbf{x}}^a_{j_1,1}) + \mathbf{b}^{d,1}(t_{1,j_1,1}) - \tfrac{1}{2h_1}\left[\tilde{\mathbf{x}}^{d,1}_{j_1+1,1} - \tilde{\mathbf{x}}^{d,1}_{j_1-1,1}\right] = 0. \tag{32}
$$

Hence the $n_1 n_2 k + n_1$ equations (29),(32) represent a nonlinear system for the unknowns $\tilde{\mathbf{x}}^{d/a}_{j_1,j_2}$ and ν_{j_1} with $j_1 = 1, \ldots, n_1$; $j_2 = 1, \ldots, n_2$. Newton's method produces an iterative solution of this system. Like in the uniform grid case, the

right-hand side of (13) has to be evaluated and the Jacobian matrices of $\mathbf{f}^{d/a}$ are required in each grid point per iteration step. We are able to calculate the dependence of the values τ_{j_1} on ν_{j_1} analytically by the polynomial approximation (23). Hence the same holds for the grid points in (27) or (28). Just the derivative of $\mathbf{b}^{d,a}$ is additionally needed, which demands one more evaluation of these functions per grid point in a numerical differentiation. Thus the effort for computing the Jacobian matrix of the whole nonlinear system increases slightly in the characteristic grid option.

6   Test Results

As benchmark, we consider a forced Van der Pol oscillator in DAE formulation

$$
\begin{array}{rcl}
\dot{x} & = & y \\
\dot{y} & = & -\gamma(x^2 - 1)y + (2\pi z)^2 x \\
0 & = & z - b(t)
\end{array}
\tag{33}
$$

with parameter γ and input signal $b(t)$. If $\gamma = 0$ and $b(t) \equiv b_0$ holds, then the system changes into a harmonic oscillator and all solutions have the frequency $\nu_0 = b_0$. For $\gamma > 0$ and $b(t) \equiv b_0$, we obtain the ordinary Van der Pol oscillator, which owns periodic steady state responses with frequency $\nu_0 < b_0$. If $b(t)$ is non-constant and periodic, the input signal introduces another time scale and causes a forced oscillator. The system (33) represents a semi-explicit DAE of index one. The unknown z can be eliminated, which yields the Van der Pol oscillator in ODE form. However, circuit simulation packages generate DAE systems, where the input signals are separated in additive form like above.

In our simulations, we choose the periodic input signal

$$
b(t) = 1 + \tfrac{1}{2} \sin\left(\tfrac{2\pi}{T_1} t\right)
\tag{34}
$$

and thus assume that the system (33) has a quasiperiodic solution of the form (8). Therefore we change to the corresponding warped MPDAE system (13). The phase condition (11) determines the local frequency function. The involved parameters are set to $\gamma = 10$ and $T_1 = 1000$.

We apply exactly the presented finite difference techniques from Sect. 4 and Sect. 5, respectively. In the latter, the characteristic grid (28) is selected. To achieve the convergence of Newton iterations, a homotopy method yields consecutive nonlinear systems corresponding to modified input signals, see [14]. Each nonlinear system is solved via the Newton-Raphson method. Since the computation of the Jacobian matrices is cheap, the computational effort consists mostly

12

	uniform grid	characteristic grid
order of Jacobian	30.100	30.100
entries in Jacobian	150.000 ($\doteq 0,02\%$)	170.600 ($\doteq 0,02\%$)
entries in LU dec.	25.001.306 ($\doteq 2,76\%$)	1.978.579 ($\doteq 0,22\%$)
CPU time for LU dec.	321 seconds	2,5 seconds
condition (1-Norm)	$2 \cdot 10^6$	$7 \cdot 10^5$

Table 1: Comparison of Jacobian matrices.

in their LU decompositions. In both finite difference methods, we arrange first the equations with discretisations of the MPDAE and then those of the phase condition. Accordingly, the unknowns contain the MVF values first and then the local frequencies. Hence the corresponding sparse Jacobian matrices exhibit the form

$$
\mathcal{J} = \left(\begin{array}{c|c} \mathcal{D} & \mathcal{N} \\ \hline \mathcal{P} & 0 \end{array} \right), \quad \begin{array}{l} \mathcal{D} \in \mathbb{R}^{n_1 n_2 k \times n_1 n_2 k} \\ \mathcal{N} \in \mathbb{R}^{n_1 n_2 k \times n_1} \\ \mathcal{P} \in \mathbb{R}^{n_1 \times n_1 n_2 k}. \end{array} \tag{35}
$$

In the simulation, we fix the grid sizes to $n_1, n_2 = 100$ for both finite difference methods. The computations have been done using MATLAB (Version 6) [10] on a workstation with Pentium III processor (733 MHz). A special solver for sparse matrices yields the LU decompositions. However, this algorithm performs only partial pivoting for numerical stability in contrast to pivoting for sparsity. Table 1 illustrates the properties of the arising Jacobian matrices in an iteration step near the final solution. The Gaussian elimination produces many fill-ins in the uniform grid case, whereas the LU decomposition stays sparse in the characteristic grid case. The resulting computation time reflects this fact. Fig. 5 shows the structure of the involved matrices, where non-zero elements are plotted. Nevertheless, the condition of both Jacobian matrices nearly coincides. Hence we can apply the cheaper option without loss of accuracy. Moreover, in the homotopy method, the total number of required Newton iteration steps is also similar in both techniques. The qualitative convergence behaviour also agrees and thus the methods have equal robustness in the test example.

Now we observe the results of our numerical simulations. Fig. 6 displays the computed local frequencies. The two finite difference techniques produce nearly the same functions. We see that the local frequency responds to the input signal. Hence the phase condition (11) is able to identify a physically correct frequency function. Accordingly, the calculated MVFs resemble in both methods, too, which is shown for the first component in Fig. 7. The other two components are given in Fig. 8 for completeness.
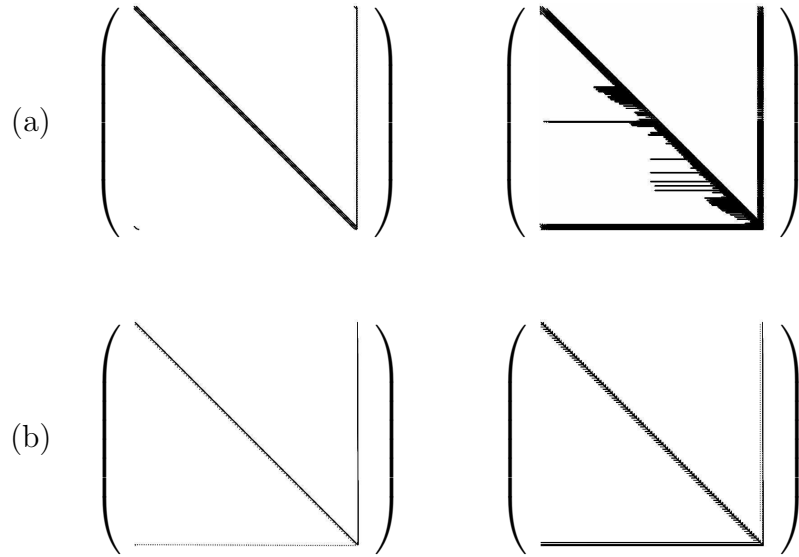
13

Figure 5: Jacobian matrices and their LU decompositions for uniform grid method (a) and characteristic grid method (b).
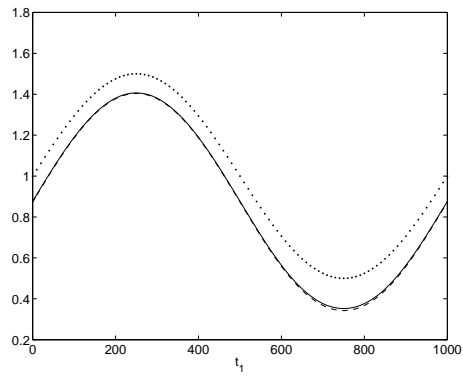

Figure 6: Local frequency computed by uniform grid option (solid line) and by characteristic grid option (dashed line), together with input signal (pointed line).
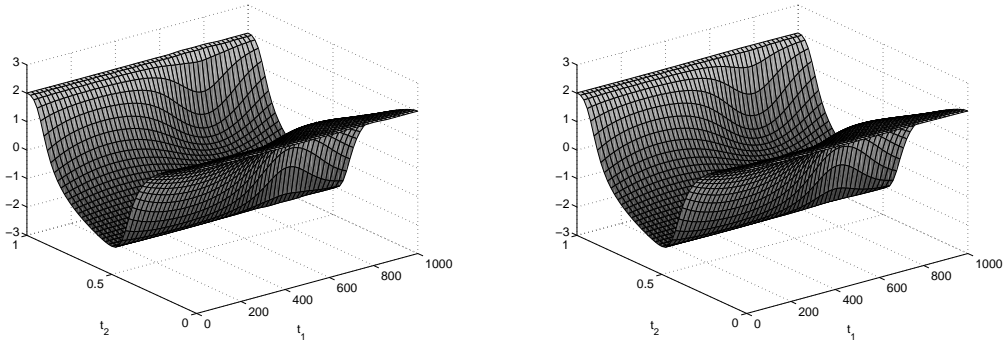
14

Figure 7: MPDAE solution for x computed by uniform grid method (left) and by characteristic grid method (right).
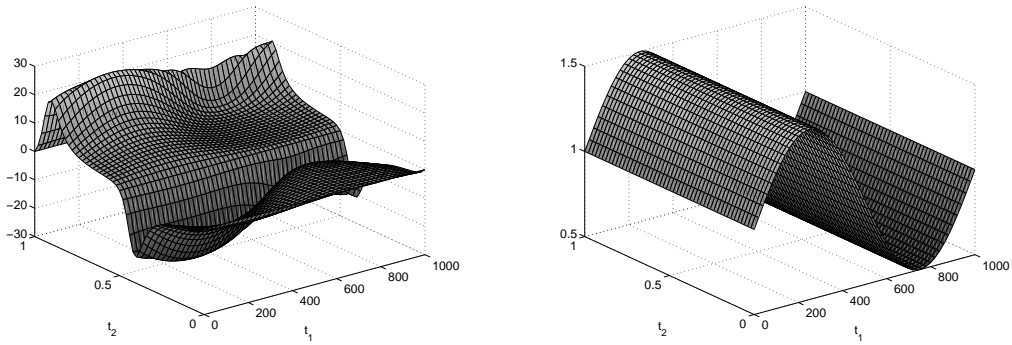

Figure 8: MPDAE solution for y (left) and z (right) obtained by characteristic grid method.
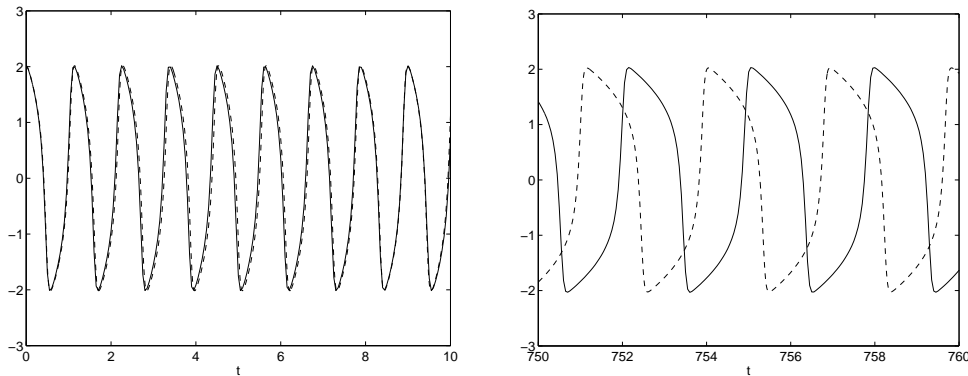
15

Figure 9: DAE solution x obtained from interpolation by MPDAE solution (solid line) and from integration of initial value problem (dashed line) in time intervals $[0, 10]$ (left) and $[750, 760]$ (right).

Finally, we reconstruct the corresponding DAE solution via (7) using interpolation by the MPDAE solution on the characteristic grid. For comparison, the DAE (33) is integrated by trapezoidal rule, where the MPDAE solution yields the initial values. Fig. 9 shows both approximations in two different time intervals. In the first few cycles, the two signals exhibit a good agreement. In later cycles, a phase shift arises due to the multidimensional model, since small numerical errors of the local frequencies amplify during many oscillations. Nevertheless, the other qualities coincide in both signals. The average frequency is $\overline{\nu} = 0.87$, which corresponds to about 870 oscillations during the period T_1. In contrast, just 100 oscillations are computed using the characteristic systems. The efficiency of the MPDAE model increases clearly for larger differing time scales, for example, if we choose a huge value T_1.

7   Conclusions

The warped MPDAE model allows an appropriate simulation of frequency modulated quasiperiodic signals including widely separated time scales. The structure of characteristic curves implies a discretisation of the MPDAE system, which produces a boundary value problem of DAEs. A finite difference method for solving this approximative system has been presented. By involving the inherent MPDAE structure, this scheme leads to extensive savings in computation time and memory in comparison to standard finite difference techniques. A numerical simulation using a benchmark system has demonstrated the applicability and efficiency of the designed method. Hence techniques based on the characteristic curves represent highly qualified schemes for solving warped MPDAE systems.

Acknowledgements

References

[1] Brachtendorf, H. G.; Welsch, G.; Laur, R.; Bunse-Gerstner, A.: Numerical steady state analysis of electronic circuits driven by multi-tone signals. Electrical Engineering 79 (1996), pp. 103-112.

[2] Eich-Soellner, E.; Führer, C.: Numerical Methods in Multibody Dynamics. Teubner, Stuttgart 1998.

[3] Günther, M.; Feldmann, U.: CAD based electric circuit modeling in industry I: mathematical structure and index of network equations. Surv. Math. Ind. 8 (1999), pp. 97-129.

[4] Günther, M.; Rentrop, P.: The differential-algebraic index concept in electric circuit simulation. Z. Angew. Math. Mech. 76 (1996) 1, pp. 91-94.

[5] Houben, S.H.M.J.: Simulating multi-tone free-running oscillators with optimal sweep following. to appear in: Proceedings Conference Scientific Computing in Electrical Engineering, Eindhoven, 2002.

[6] John, F.: Partial Differential Equations. 4th Ed., Springer, New York 1982.

[7] Kampowsky, W.; Rentrop, P.; Schmitt, W.: Classification and numerical simulation of electric circuits. Surv. Math. Ind. 2 (1992), pp. 23-65.

[8] Kundert, K. S.; Sangiovanni-Vincentelli, A.; Sugawara, T.: Techniques for finding the periodic steady-state response of circuits. In: Ozawa, T. (Ed.): Analog methods for computer-aided circuit analysis and diagnosis. New York 1988, pp. 169-203.

[9] Lamour, R.; Lentini, M.; März, R.: The condition of boundary value problems in transferable differential-algebraic equations and shooting methods. Preprint Nr. 91-19, Department of Mathematics, Humboldt Universität Berlin 1991.

[10] The MathWorks, Inc.: Using MATLAB (Version 6). Ed. 2000.

[11] Narayan, O.; Roychowdhury, R.: Analyzing oscillators using multitime PDEs. IEEE Trans. CAS I 50 (2003) 7, pp. 894-903.

[12] Pulch, R.; Günther, M.: A method of characteristics for solving multirate partial differential equations in radio frequency application. Appl. Numer. Math. 42 (2002), pp. 397-409.

[13] Pulch, R.: Finite difference methods for multi time scale differential algebraic equations. Z. Angew. Math. Mech. 83 (2003) 9, pp. 571-583.

[14] Pulch, R.: Multi Time Scale Differential Equations for Simulating Frequency Modulated Signals. to appear in: Appl. Numer. Math.

[15] Rentrop, P.; Strehmel, K.; Weiner, R.: Ein Überblick über Einschrittverfahren zur numerischen Integration in der technischen Simulation. GAMM-Mitt. 19 (1996) 1, pp. 9-43.

[16] Roychowdhury, J.: Analysing circuits with widely-separated time scales using numerical PDE methods. IEEE Trans. CAS I 48 (2001) 5, pp. 578-594.